RSC Advances

PAPER

View Article Online
View Journal | View Issue



Cite this: *RSC Adv.*, 2017, **7**, 46657

# Detection of phosphate based on phosphorescence of Mn doped ZnS quantum dots combined with cerium(III)†

Jin Qin, Dongxia Li, Yanming Miao and Guiqin Yan *

Received 20th July 2017
Accepted 28th September 2017

DOI: 10.1039/c7ra07991e

rsc.li/rsc-advances

A simple and rapid room-temperature phosphorescence (RTP) sensor for phosphate detection was developed on the basis of $Ce^{3+}$ modulated mercaptopropionic acid (MPA)-capped Mn-doped ZnS quantum dots (QDs). This sensor utilizes the affinity of lanthanides-phosphates and the RTP properties of doped QDs. $Ce^{3+}$ can electrostatically interact with carboxyl groups on the surface of MPA-capped Mn-doped ZnS QDs, which leads to the aggregation of QDs and changes the RTP signals. The high affinity of phosphate to $Ce^{3+}$ enables the dissociation of $Ce^{3+}$ from the surface of MPA-capped ZnS QDs, forming a stable complex with phosphate and recovering the RTP of the QDs. Under the optimized conditions, the phosphate detection range is 8 to 320 μM ($R$ = 0.9998) and the detection limit is 2.71 μM. Thus, the new sensor is potential for phosphate detection in environmental water without complicated pretreatment and is free from the interference of background fluorescence or scattering light.



## 1. Introduction

Eutrophication has become a global environmental problem in stagnant water bodies such as lakes, reservoirs, and estuaries. Phosphates are a group of well-known contaminants in ground and surface water, and the excess of phosphates usually leads to excessive algal growth followed by decomposition, depletion in dissolved oxygen, eutrophication, reduction in water quality[1,2] and even the release of secondary metabolites of biotoxins. These harmful algal blooms can devastate local ecosystem, the fishing industry, water sports and leisure activities, and drinking water supply.[3] In the natural water body without eutrophication, the limit standard of phosphate environmental quality was 0.02 mg $L^{-1}$.[4] Therefore, phosphate detection is of great significance for the control and guard of eutrophication. Up to now, many methods have been developed for quantitative analysis of phosphate, including colorimetry,[5,6] fluorimetry,[7–9] chromatography[10] electrochemical method[11,12] and enzymatic biosensors.[13] However, further application of new methods is hampered due to the great time consumption, high cost and complicated pretreatment. Thus, development of sensitive, reliable and easy phosphate detection method is still highly demanded.

Room-temperature phosphorescence (RTP) quantum dots (QDs) become a research hotspot in the field of optical sensors and are widely used to prepare different sensors.[14–30] Owing to long lifetime and appropriate delay, RTP reserves high intensity after the termination of matrix fluorescence attenuation, and thus can avoid the interference of the background fluorescence and scattering light from other fluorescent substances.[14,18] Moreover, since RTP is less frequent than fluorescence, RTP sensors are significantly more selective[14] and no complex pretreatment is needed.[18,23] Thus, the RTP of Mn-doped ZnS (Mn-ZnS) QDs can be utilized to detect environmental pollutants.

Owing to the high affinity with phosphates/phosphate esters, trivalent lanthanide ions are widely used to develop sensors for detection of physiological phosphates and phosphate-containing biomolecules.[31–34] $Ce^{3+}$ is the most abundant among rare earth elements and is superior with lower costs and accessible raw materials. Since $Ce^{3+}$ is more affine to phosphates,[35] $Ce^{3+}$ will be potentially and widely used to detect phosphate pollutants in the environment.

In this study, we prepared the $Ce^{3+}$/MPA-capped Mn-ZnS QDs nanohybrids and used them as an RTP sensor for phosphate detection. The principles of our phosphate sensing concept are shown in Fig. 1, Initially, $Ce^{3+}$ ions can coordinate to the carboxylate groups on the surface of the MPA-capped Mn-ZnS QDs,[36] where they act as a bridge for the induction of Mn-ZnS QDs aggregation. After phosphates were added to this system, the stronger interaction between phosphates and $Ce^{3+}$ would result in the formation of more-stable hybrids, which competitively desorbed the $Ce^{3+}$ from the surfaces of Mn-ZnS QDs, thus dispersing the Mn-ZnS-QDs/$Ce^{3+}$ nanohybrids and restoring the RTP of Mn-ZnS QDs. Based on this principle, we built a phosphate phosphorescence detection sensor. This sensor is featured by simple operations and a wide detection range, and

*Shanxi Normal University, Linfen, Shanxi 041000, China. E-mail: gqyan2013@163.com; Fax: +86-0357-2051249*

† Electronic supplementary information (ESI) available. See DOI: 10.1039/c7ra07991e

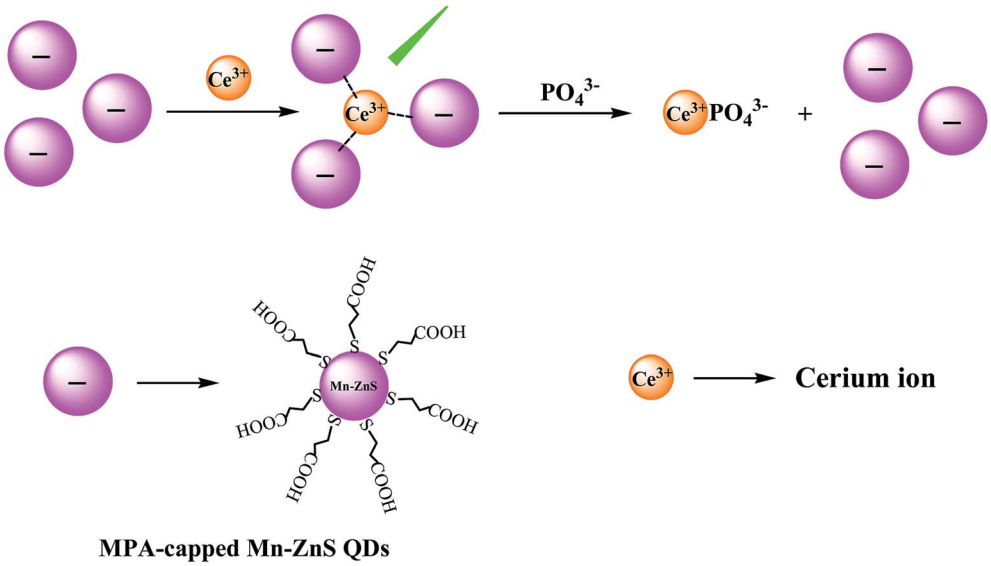


Fig. 1 Design of phosphate sensors based on Mn-ZnS-QDs/$Ce^{3+}$ nanohybrids.

avoids the interferences from background fluorescence and scattering light. Besides, when used to detect the phosphates in real water, this sensor does not need complex pretreatment and thus is more practicable.

## 2. Materials and methods

### 2.1 Materials and apparatus

Mn-doped ZnS QDs were prepared from mercaptopropionic acid (MPA; J&K Scientific, Beijing, China), $Mn(Ac)_2 \cdot 4H_2O$, $Zn(Ac)_2 \cdot 2H_2O$ and $Na_2S \cdot 9H_2O$ (Tianjing Kermel Chemical Reagent Co., China). Ultrapure water (18.2 MΩ cm) was generated from a Water Pro water purification system (Labconco Corporation, Kansas City, MO). $Ce(NO_3)_3 \cdot 6H_2O$ and $Na_3PO_4$ were purchased from Sigma Corporation of America.

The morphology and microstructure of the QDs were characterized on a JSM-7500F transmission electron microscope (TEM, Japan). Phosphorescence was measured on a Cary Eclipse fluorescence spectrophotometer (Varian American Pty Ltd., America) in the phosphorescence mode, equipped with a plotter unit and a quartz cell ($1 \times 1$ $cm^2$). The slits for excitation and emission were both 10 nm wide. Ultraviolet/visible (UV/vis) absorption spectra were recorded using a Shimadzu UV-29100 UV/vis spectrophotometer. The pH meter was bought from Jinpeng Analytical Instruments Co. Ltd. (China). Rotatory evaporator was bought from Shanghai Yarong Instruments Co. Ltd. (China).

### 2.2 Synthesis of the Mn-doped ZnS QDs

The MPA-capped Mn Doped ZnS QDs were synthesized according to references with some modification.[19,26] Briefly, a colloidal solution was synthesized in a 250 mL three-neck flask with pH electrodes, followed by addition of 180 μL of 0.04 M MPA, 5 mL of 0.1 M $Zn(Ac)_2$, and 2 mL of 0.01 M $Mn(Ac)_2$. The mixture was adjusted to pH 11 with 1 M NaOH and stirred under argon bubbling at room temperature for 30 min. Then 5 mL of 0.1 M $Na_2S$ was quickly injected into the solution under isolation from air. After 20 min of stirring, the solution was aged at 50 °C in open air for 2 h to form MPA-capped Mn-doped ZnS QDs. As for purification, the QDs were precipitated with the same volume of ethanol, centrifuged, washed with ethanol, and vacuum-dried at room temperature. The QD powder as-obtained was highly water-soluble.

### 2.3 Analytical procedures

**2.3.1 Effects of $Ce^{3+}$ on the RTP intensity of Mn-ZnS QDs.** To study the effect of $Ce^{3+}$ on the RTP intensity of MPA-capped Mn-doped ZnS QDs, we first dissolved $Ce(NO_3)_3$ in water to form a 40 μM solution. Second, a series of samples was prepared by adding different amounts of $Ce^{3+}$ to Tris–HCl buffer (pH 7.4, 20 mM). Third, the MPA capped Mn-doped ZnS QDs were dissolved in water to a concentration of 2 mg $mL^{-1}$, and then 100 μL of the QDs solution was added to each of the above $Ce^{3+}$ solutions. After 5 min at room temperature, the phosphorescence at an excitation wavelength of 295 nm was measured.

**2.3.2 Phosphorescence response between ZnS/$Ce^{3+}$ and phosphates.** For phosphate determination, phosphate was dissolved in water to form a 10 mM solution. The assay solutions containing MPA-capped Mn-doped ZnS QDs (100 μL), $Ce^{3+}$ (4 μM), and various concentrations of phosphate (0–1600 μM) were prepared in 500 μL of Tris–HCl buffer (pH 7.4, 20 mM). Reactions were performed for 5 min before spectrophotometric analysis.

**2.3.3 Sample detection.** Water samples were collected from Fen River located (a branch of Yellow River in china) and lake of Yuxiu (Shanxi Normal University in china). The samples were filtered through a 0.45 μm membrane filter, rotationally evaporated, and concentrated 30 times before analysis. Each experiment was conducted in triplicate. The water samples were added with different amount of a phosphate solution. The

 

feasibility of this method was validated through spiked recovery trials.

## 3. Results and discussion

### 3.1 Characterization of MPA-capped Mn-doped ZnS QDs

The size of Mn-ZnS QDs observed by TEM is about 3.5 nm (Fig. S1a†). The maximum excitation peak is 295 nm and the maximum emission peak is 590 nm; where $hv_1$ is the fluorescence induced by ZnS surface defects; $hv_2$ is the phosphorescence caused by the $Mn^{2+}$ $^4T_1$–$^6A_1$ transition (Fig. S1b†). After the ZnS matrix absorbed the excitation light, the holes were captured by $Mn^{2+}$, while the electrons and holes separately compounded on $Mn^{2+}$, leading to the stimulation of $Mn^{2+}$ and finally forming an orange RTP emission (about 590 nm).[37,38]

### 3.2 Construction of Mn-ZnS QDs/$Ce^{3+}$ sensor

As reported, some metal ions can efficiently induce the change of quantum photoluminescence.[39–41] We first observed how $Ce^{3+}$ would affect the RTP emission spectrum of Mn-ZnS QDs (Fig. 2). After $Ce^{3+}$ was added into the Mn-ZnS QD solution, the RTP intensity of the Mn-ZnS QDs was enhanced with the increase of $Ce^{3+}$ concentration and was maximized at the concentration of 4 μM $Ce^{3+}$(Fig. 2a). Interestingly, when the $Ce^{3+}$ concentration was above 4 μM, the RTP intensity of Mn-ZnS QDs stopped increasing, but declined (Fig. 2b). The RTP intensity of nanohybrids formed by $Ce^{3+}$ and Mn-doped ZnS QDs is 10.4 times as large as that of Mn-doped ZnS QDs at the same concentration (Fig. 2c). This phenomenon indicates the high effects of the concentrations of $Ce^{3+}$ and Mn-doped ZnS QDs on the RTP intensity of the nanohybrids. Thereby, we deduce this phenomenon is mainly attributed to the $Ce^{3+}$-induced QDs aggregation. Since the excess of $Ce^{3+}$ would affect the systematic response and given the stability and sensitivity of the detection system, we selected the concentration of 4 μM $Ce^{3+}$ in the subsequent trials.

### 3.3 Principle of Mn-ZnS-QDs/$Ce^{3+}$ sensor construction

The MPA that capped the surfaces of Mn-ZnS QDs not only enhanced the water-solubility of the QDs, but also endowed the dot surfaces with abundant carboxyl. Thereby, the $Ce^{3+}$ could coordinately complex with the surface carboxyl, forming Mn-ZnS QDs/$Ce^{3+}$ nanohybrids, leading to the aggregation of QDs. The dot surface defects induced by electrons–holes would generate a local electric field.[42,43] After the addition of $Ce^{3+}$, the distances between the Mn-ZnS QDs were shortened, which enhanced the Coulomb force of Mn-ZnS QDs. As a result, the local electric field around the QDs was enhanced, which induced the QDs to produce more-effective excitation,[44] so more energy was transferred from the surface holes of Mn-ZnS QDs to $Mn^{2+}$ and finally the RTP intensity of Mn-ZnS QDs was significantly enhanced.[17,45] However, the number of carboxyl binding

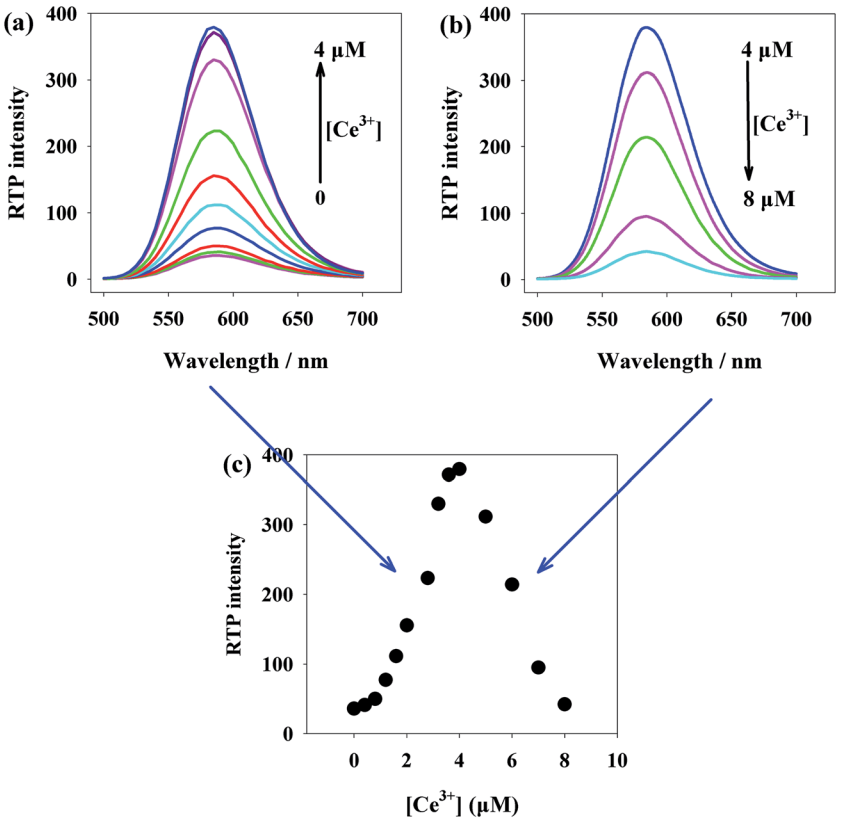


Fig. 2 $Ce^{3+}$ concentration-dependent RTP emission of the MPA-capped Mn-doped ZnS QDs. (a, b) The change of the RTP intensity with the increase of the concentration of $Ce^{3+}$; (c) the plot of RTP intensity with the increase of the concentration of $Ce^{3+}$.

sites on the surfaces of the QDs was finite, so when the $Ce^{3+}$ concentration around the QDs was saturated, the QDs would be dispersed (Fig. 3a).

When two substances aggregate through interaction and produce scattering particles, they can generate very remarkable resonance light scattering (RLS) signals. By analyzing the RLS spectrum of $Ce^{3+}$ and Mn-ZnS QDs interaction, we find the Mn-ZnS QDs emitted low RLS within the wavelength of 200–700 nm. However, after $Ce^{3+}$ was slowly added into the Mn-ZnS QDs solution, the RLS intensity in the reaction system was gradually enhanced (maximum absorption peak was 395 nm) (Fig. 3b), indicating the Mn-ZnS QDs and $Ce^{3+}$ interacted to form larger scattering particles. With the increase of $Ce^{3+}$ concentration above 4 μM, the RLS intensity in the reaction system was gradually weakened (Fig. 3c), indicating the QDs were dissociated. The Mn-ZnS QDs and $Ce^{3+}$ aggregated due to electrostatic attraction, but the QDs were dissociated when the $Ce^{3+}$ concentration around the QDs was saturated. Further ultraviolet spectral analysis shows that with the increase in $Ce^{3+}$ concentration, the absorption peaks of MPA-capped Mn-ZnS QDs within 240–360 nm were gradually enhanced (Fig. 3d), which validate the interaction between $Ce^{3+}$ and Mn-ZnS QDs.

### 3.4 Influence factors on stability of Mn-ZnS QDs/$Ce^{3+}$ nanohybrids

To enhance the stability and selectivity of the new sensor during phosphate detection, we investigated the effects of pH, reaction

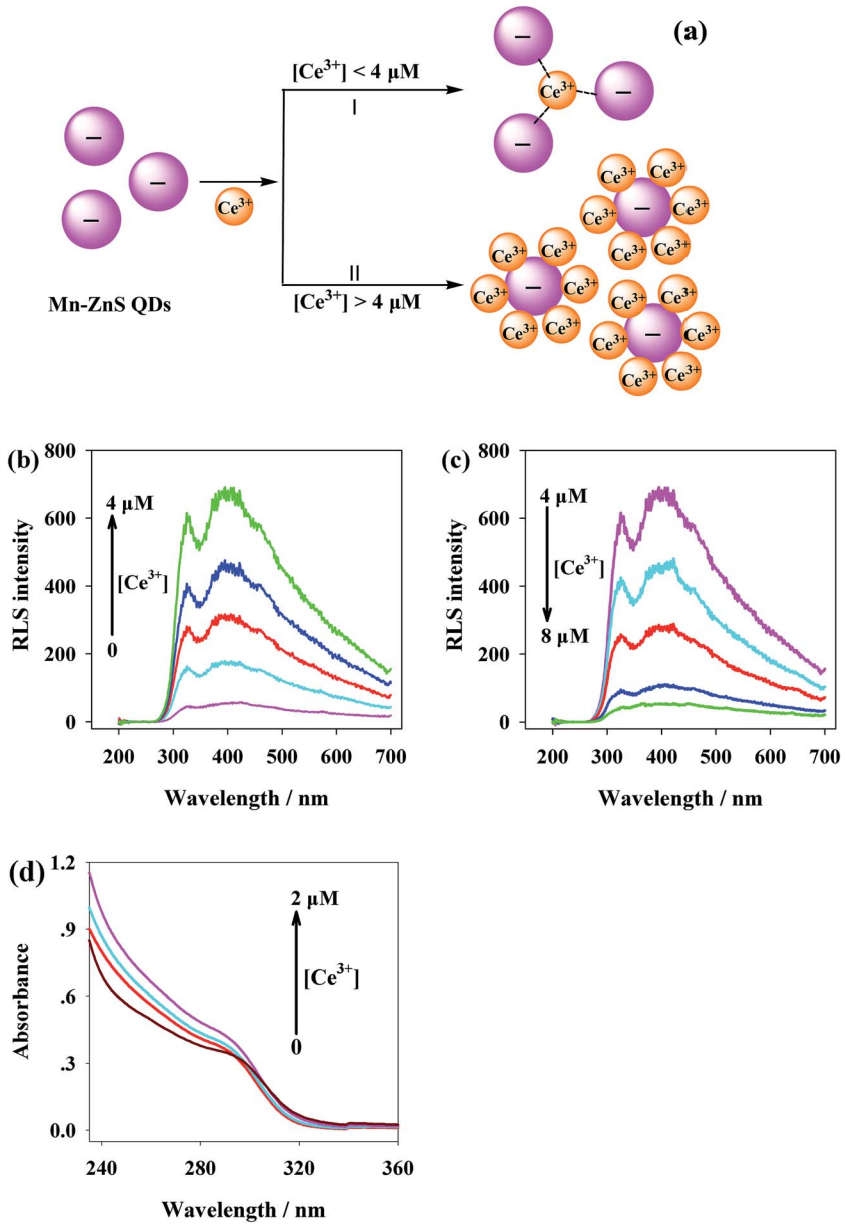


Fig. 3 (a) Schematic illustration of fabricating Mn-ZnS QDs after the addition of $Ce^{3+}$; (b, c) RLS spectra of the Mn-ZnS QDs in the presence of different concentrations of $Ce^{3+}$; (d) the absorption spectra of QDs in the presence of various concentrations of $Ce^{3+}$.

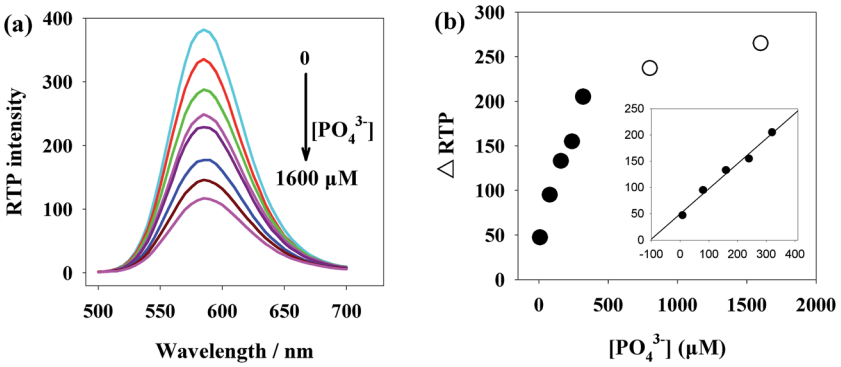


Fig. 4 (a) Phosphate concentration-dependent RTP emission of the Mn-ZnS QDs/$Ce^{3+}$. (b) The relationship between ΔRTP and the phosphate concentration.

time and salt concentrations. As showed in Fig. S2a,† within pH 6.5–7.5, the RTP intensity of the three reaction systems stabilized. Given the precipitation of rare earth ions under base conditions, we selected the pH 7.4 in the following measurements. Meanwhile, the Mn-ZnS QDs/$Ce^{3+}$ nanohybrids within 60 min and under the high concentration of salts basically were maintained stable.

### 3.5 Detection of phosphate by Mn-ZnS/$Ce^{3+}$ nanohybrids

Under the above optimal conditions, we studied the relationship between the RTP intensity of Mn-ZnS QDs/$Ce^{3+}$ nanohybrids and the phosphate concentration. As showed in Fig. 4a, with the rise of phosphate concentration, the RTP intensity of the Mn-ZnS QDs/$Ce^{3+}$ nanohybrids was regularly quenched, indicating the RTP sensor of Mn-ZnS QDs/$Ce^{3+}$ nanohybrids can be used to detect phosphates. The linearity between the RTP quenching value of Mn-ZnS QDs/$Ce^{3+}$ nanohybrids (ΔRTP) and the phosphate concentration under the optimal conditions was obtained (Fig. 4b).

Fig. 5a shows the UV-vis spectra of phosphate (curve 1), $Ce^{3+}$ (curve 2) and Mn-ZnS QDs (curve 3). With the addition of $Ce^{3+}$, the spectra of the Mn-ZnS QDs were enhanced (curve 4). With the addition of phosphate into the Mn-ZnS QDs and $Ce^{3+}$ mixed solution, the ultraviolet spectra of the Mn-ZnS QDs were further enhanced and red-shifted (curve 5). These changes indicate there is interaction between the Mn-ZnS QDs and $Ce^{3+}$ and between phosphate and Mn-ZnS QDs/$Ce^{3+}$ nanohybrids. The ultraviolet spectra of $Ce^{3+}$/phosphate binding (Fig. 5b) show that the UV intensity of single phosphate was very weak, and with the rise of $Ce^{3+}$ concentration within 0–2 μM, the UV absorption intensity of the phosphate was gradually enhanced and significantly red-shifted, indicating the $Ce^{3+}$ and phosphate formed larger scattering particles.

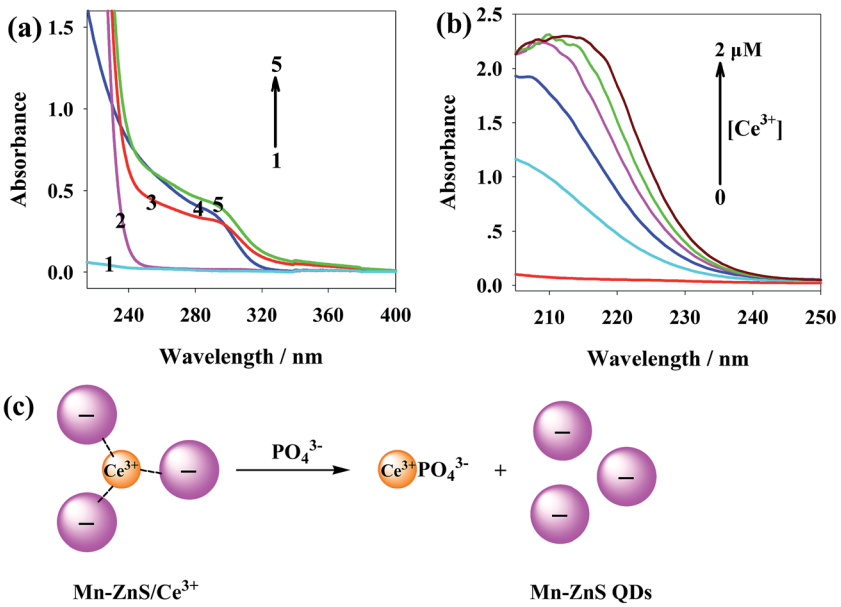


Fig. 5 (a) UV-vis absorption spectra of (1) phosphate, (2) $Ce^{3+}$, (3) Mn-ZnS QDs, (4) Mn-ZnS QDs/$Ce^{3+}$ nanohybrids, (5) Mn-ZnS QDs/$Ce^{3+}$+ phosphate; (b) absorption spectra of phosphate in the presence of different concentrations of $Ce^{3+}$; (c) schematic illustration of fabricating Mn-ZnS QDs/$Ce^{3+}$ after the addition of phosphate.

Table 1 Comparison of the proposed method with different analytical techniques reported for detection of phosphate

| Sensing matrix | Line arrange (μM) | Limiting detection (μM) | Ref. |
|---|---|---|---|
| AuNPs based colorimetric method | 0.5–30 | 0.076 | 4 |
| AuNPs based colorimetric method | — | 120 | 5 |
| Fluorescence method | 0.33–5 | 0.025 | 8 |
| Electrochemica method | 2.5–130 | 2 | 12 |
| Phosphorescent method | 8–320 | 2.71 | This work |

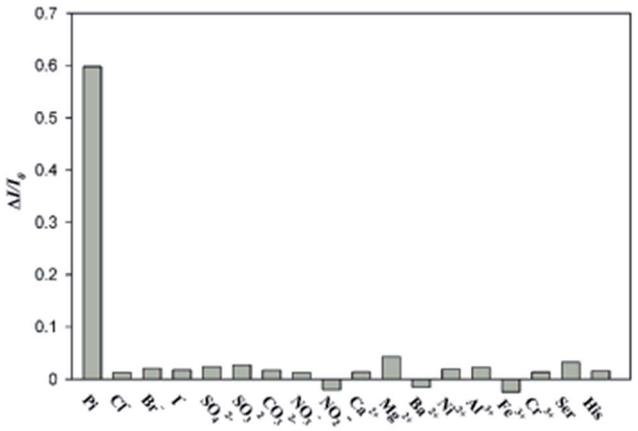


Fig. 6 Selectivity of the RTP assay for phosphate over other substances. The concentration of phosphate was 100 μM and that of other substances was 2000 μM.

As showed in Fig. 5c, the addition of $PO_4^{3-}$ significantly reduced the clustering of QDs. Though $Ce^{3+}$ could bind with carboxyl, $Ce^{3+}$ was more affine to phosphates.[34] As reported, the complexation constant between $PO_4^{3-}$ and $Ce^{3+}$ was far larger than that between carboxyl and $Ce^{3+}$.[46,47] Thus, the addition of phosphates destroyed the aggregation of the Mn-ZnS QDs/$Ce^{3+}$ nanohybrids, and the phosphate and $Ce^{3+}$ formed more-stable hybrids, which dispersed the QDs to the solution again and recovered the phosphorescence. Given that phosphates could restore the RTP intensity of the reaction system, we thereby built a novel RTP sensor for phosphate detection.

Under the optimal conditions, this new sensor has high linearity in phosphate detection within the range of 8–320 μM, with a linear equation of $\Delta RTP = 78.4x - 73.6$ ($R = 0.9998$) and a detection limit of $3\sigma = 2.71$ μM. We continuously detected both a phosphate-free solution and a 80 μM phosphate solution for 11 times, and got the relative standard deviation of 3.1%. Compared with other phosphate measurement methods (Table 1), this new sensor has a detection limit lower than colorimetry,[6] higher than AuNPs based colorimetric method,[5] fluorescence method[9] and electrochemical method,[13] but its linear range is broader than these methods. Besides, the phosphorescence detection system efficiently avoids the interferences from background fluorescence and scattering light. Moreover, the QDs-based RTP method does not need deoxidant or other inducers and sophisticated electrode modification. Thus, this method is more feasible for phosphate detection in complex water samples.

### 3.6 Interferences from coexisting substances

Considering the promise of the Mn-ZnS QDs/$Ce^{3+}$ sensor system for application in environmental fields, the selectivity of the phosphorescence sensor for phosphate was evaluated. This was achieved by monitoring the RTP responses of the Mn-ZnS QDs/$Ce^{3+}$ complex upon addition of phosphate and some coexisting substances, including anions such as $Cl^-$, $Br^-$, $I^-$, $SO_4^{2-}$, $SO_3^{2-}$, $CO_3^{2-}$, $NO_3^-$, $NO_2^-$, cations such as $Ca^{2+}$, $Mg^{2+}$, $Ba^{2+}$, $Ni^{2+}$, $Al^{3+}$, $Fe^{3+}$, $Cr^{3+}$, and amino acids such as serine (Ser), histidine (His), all of which were kept at a concentration twenty times higher than that of phosphate. As shown in Fig. 6, phosphate can significantly restore the RTP intensity of the Mn-ZnS QDs/$Ce^{3+}$ complex in the presence of all potential competitors tested. In contrast, no clear enhancement is observed with any other ions or amino acids. The results demonstrate that this RTP probe is highly selective for phosphate. This high specificity could be attributed to the specific and robust affinity between $Ce^{3+}$ ions and phosphate. These properties are important for investigating environmental samples.

### 3.7 Sample analysis

The excellent specificity combined with high sensitivity and fast response of the Mn-ZnS QDs/$Ce^{3+}$ complex to phosphate suggests that this method might be directly applied to detecting phosphate in real samples. Therefore, we examined the practicality of the assay for phosphate detection in environmental. Water samples were collected from Fen River, Yuxiu lake. The samples were filtrated with 0.45 μm filter, rotationally evaporated, and concentrated 30 times before analysis. The

Table 2 Concentrations of phosphates in real water samples ($n = 3$)

| Water samples | Ammonium molybdate method (μM) | Spiked (μM) | Measured (μM) | RSD (%) | Recovery (%) |
|---|---|---|---|---|---|
| Fenhe | 0.5 | 0 | 0.6 | 4.12 | — |
| | 76.1 | 80 | 74.5 | 3.06 | 92.4 |
| | 163.4 | 160 | 171.2 | 2.87 | 106.6 |
| Yuxiu lake | 3.1 | 0 | 2.9 | 3.74 | — |
| | 87.2 | 80 | 86.3 | 3.43 | 104.2 |
| | 155.3 | 160 | 153.7 | 2.45 | 94.3 |

concentration of phosphate was determined experimentally (Table 2). Clearly, when this sensor was used to detect phosphate concentrations in real water samples, the spiked recovery rates were 92.4–106.6%, indicating the detections were reliable.

## 4. Conclusions

We designed a simple and rapid phosphate RTP sensor. This sensor eliminated complex sample pretreatment and avoided the interferences of background fluorescence and scattering light from fluorescent substances. The example of the use of ZnS QDs was environmentally friendly and easily prepared. With high sensitivity and wide linear range, this sensor can be promising as versatile probes in the environmental in the future.

## Conflicts of interest

There are no conflicts to declare.

## Acknowledgements

This work was supported by the Research Fund for the Doctoral Program of Higher Education of China (NO. 20111404110002). Fund for Construction Program of Chemical Advantage and Key Discipline of Shanxi Province of China (NO. 912019).

## References

1 C. Warwick, A. Guerreiro and A. Soares, *J. Biosens. Bioelectron.*, 2013, **41**, 1–11.
2 A. T. Law al and S. B. Adeloju, *Talanta*, 2013, **114**, 191–203.
3 J. Heisler, P. M. Glibert, J. M. Burkholder, D. M. Anderson, W. Cochlan, W. C. Dennison, Q. Dortch, C. J. Gobler, C. A. Heil, E. Humphries, A. Lewitus, R. Magnien, H. G. Marshall, K. Sellner, D. A. Stockwell, D. K. Stoecker and M. Suddleson, Eutrophication and harmful algal blooms: a scientific consensus, *Harmful Algae*, 2008, **8**, 3–13.
4 USEPA, *Nutrient Criteria Technical Guidance Manual, Office of Science and Technology*, U.S. EPA, Washington, DC, 2000.
5 W. Liu, Z. Du, Y. Qian and F. Li, *Sens. Actuators, B*, 2013, **176**, 927–931.
6 G. He, L. Zhao, K. Chen, Y. Liu and H. Zhu, *Talanta*, 2013, **106**, 73.
7 H. X. Zhao, L. Q. Liu, Z. D. Liu, Y. Wang, X. J. Zhao and C. Z. Huang, *Chem. Commun.*, 2011, **47**, 2604–2606.
8 J. M. Bai, L. Zhang, R. P. Liang and J. D. Qiu, *Chem.– Eur. J.*, 2013, **19**, 3822–3826.
9 M. R. Ganjali, M. Hosseini, Z. Memari, F. Faridbod, P. Norouzi, H. Goldooz and A. Badiei, *Anal. Chim. Acta*, 2011, **708**, 107–110.
10 M. Colina and P. H. E. Gardiner, *J. Chromatogr. A*, 1999, **847**, 285–290.
11 W. H. Lee, Y. Seo and P. L. Bishop, *Sens. Actuators, B*, 2009, **137**, 121–128.
12 W. L. Cheng, J. W. Sue, W. C. Chen, J. L. Chang, J. M. Zen and A. Chem, *J. Anal. Chem.*, 2010, **82**, 1157.
13 L. Gilbert, A. T. A. Jenkins, S. Browning and J. P. Hart, *Sens. Actuators, B*, 2011, **160**, 1322–1327.
14 J. M. Costa-Fernández, R. Pereiro and A. Sanz-Medel, *TrAC, Trends Anal. Chem.*, 2006, **25**, 207–218.
15 J. M. Traviesaalvarez, I. Sánchezbarragán, J. M. Costafernández, R. Pereiro and A. Sanzmedel, *Analyst*, 2007, **132**, 218–223.
16 Y. He, H. F. Wang and X. P. Yan, *J. Anal. Chem.*, 2008, **80**, 3832–3837.
17 Y. He, H. F. Wang and X. P. Yan, *Chem.–Eur. J.*, 2009, **15**, 5436–5440.
18 P. Wu, Y. He, H. F. Wang and X. P. Yan, *J. Anal. Chem.*, 2010, **82**, 1427–1433.
19 W. S. Zou, D. Sheng, X. Ge, J. Q. Qiao and H. Z. Lian, *J. Anal. Chem.*, 2011, **83**, 30–37.
20 P. Wu, L. N. Miao, H. F. Wang, X. G. Shao and X. P. Yan, *Angew. Chem., Int. Ed.*, 2011, **50**, 8118–8121.
21 C. X. Yang and X. P. Yan, *J. Anal. Chem.*, 2011, **83**, 7144–7150.
22 H. B. Ren and X. P. Yan, *Talanta*, 2012, **97**, 16–22.
23 E. Sotelo-Gonzalez, M. T. Fernandez-Argüelles, J. M. Costa-Fernandez and A. Sanz-Medel, *Anal. Chim. Acta*, 2012, **712**, 120–126.
24 H.-F. Wang, Y.-Y. Wu and X.-P. Yan, *J. Anal. Chem.*, 2013, **85**, 1920–1925.
25 P. Wu and X. P. Yan, *Chem. Soc. Rev.*, 2013, **2013**(42), 5489.
26 Y. Miao, Z. Zhang, Y. Gong and G. Yan, *J. Biosens. Bioelectron.*, 2014, **59**, 300–306.
27 Y. Miao, Z. Zhang, Y. Gong, Q. Zhang and G. Yan, *J. Biosens. Bioelectron.*, 2014, **52**, 271–276.
28 P. Wu, T. Zhao, J. Zhang, L. Wu and X. Hou, *J. Anal. Chem.*, 2014, **86**, 10078–10083.
29 P. Wu, J. Zhang, S. Wang, A. Zhu and D. X. Hou, *Chem.– Eur. J.*, 2014, **20**, 952–956.
30 P. Wu, T. Zhao, Y. Tian, L. Wu and D. X. Hou, *Chem.–Eur. J.*, 2013, **19**, 7473–7479.
31 J. Massue, S. J. Quinn and T. Gunnlaugsson, *J. Am. Chem. Soc.*, 2008, **130**, 6900.
32 E. A. Weitz, J. Y. Chang, A. H. Rosenfield and V. C. Pierre, *J. Am. Chem. Soc.*, 2012, **134**, 16099.
33 S. Nadella, J. Sahoo, P. S. Subramanian, A. Sahu, S. Mishra and M. Albrecht, *Chem.–Eur. J.*, 2014, **20**, 6047–6053.
34 M. Schäferling and O. S. Wolfbeis, *Chem.–Eur. J.*, 2007, **13**, 4342–4349.
35 R. Samy, P. J. Faustino, W. Adams, L. Yu, M. A. Khan and Y. Yang, *J. Pharm. Biomed. Anal.*, 2010, **51**, 1108–1112.
36 H. S. Huh and S. W. Lee, *Bull. Korean Chem. Soc.*, 2006, **27**, 1839–1843.
37 R. Thakar, Y. Chen and P. T. Snee, *Nano Lett.*, 2007, **7**, 3429.
38 J. H. Chung, C. S. A. And and D. J. Jang, *J. Phys. Chem. B*, 2001, **105**, 4128–4132.
39 Y. Gong and Z. Fan, *J. Biosens. Bioelectron.*, 2015, **66**, 533–538.
40 Z. Zhang, Y. Miao, L. Lian and G. Yan, *Anal. Biochem.*, 2015, **489**, 17–24.
41 Y. Shen, S. Liu, J. Yang, L. Wang, X. Tan and Y. He, *Sens. Actuators, B*, 2014, **199**, 389–397.

42 D. J. Norris, A. Sacra, C. B. Murray and M. G. Bawendi, *Phys. Rev. Lett.*, 1994, **72**, 2612–2615.
43 V. I. Klimov, *J. Phys. Chem. B*, 2000, **104**, 6112–6123.
44 O. Kulakovich, N. Strekal, A. Yaroshevich, S. Maskevich, S. Gaponenko, I. Nabiev, A. Ulrike Woggon and M. Artemyev, *Nano Lett.*, 2002, **2**, 1449–1452.
45 Y. Hou, J. Ye, Z. Gui and G. Zhang, *Langmuir*, 2008, **24**, 9682–9685.
46 J. Galea, R. Beccaria, G. Ferroni and J. P. Belaich, *Electrochim. Acta*, 1978, **23**, 647–652.
47 J. E. Powell, J. L. Farrell, W. F. S. Neillie and R. Russell, *J. Inorg. Nucl. Chem.*, 1968, **30**, 2223–2231.